Unveiling the Dynamics of Mantle Plumes Initiated by Rayleigh-Taylor Instabilities: Impact of Layer-Parallel Global Flows

Arnab Roy, Dip Ghosh and **Nibir Mandal**

Jadavpur University, India

AGU23 San Francisco, CA & Online Everywhere 11-15 December 2023

Abstract and Motivation

Mantle plumes arising from deep sources in the Earth are thought to have played a critical role in determining the planetary geodynamics. The plumes originate mostly from gravitational or thermochemical instabilities at the core-mantle boundary, triggered by density fluctuations due to thermal or chemical variations. Understanding the initiation mechanics of such instabilities is a key step to comprehending the formation of these deep-mantle plumes, reflected from hotspots scattered over the globe. Previous studies have explained their growth within a theoretical framework of Rayleigh-Taylor (RT) instabilities. However, a critical aspect that has been largely overlooked is the potential influence of layer-parallel global flows on the dynamics and initiation processes of instabilities. The present study combines 2D finite element particle-in-cell numerical simulations with a linear stability analysis to show the impact of global flows on the growth kinematics of RT instabilities in a thermal boundary layer at the core-mantle boundary. The simulation results indicate that the global flow acts as a counter factor to dampen their growth rates. At a threshold global flow velocity the dampening effects completely suppress the instabilities, allowing the entire system to advect in the horizontal direction. The stability analysis also predicts a non-linear increase in the instability wavelength with increasing global flow velocity. The new finding implies that the spatial frequency of plumes can remarkably drop in kinematically active regions of Earth's mantle. The presentation finally offers a possible explanation for unusually large spacing between major hotspots scattered around the globe in the light of instability

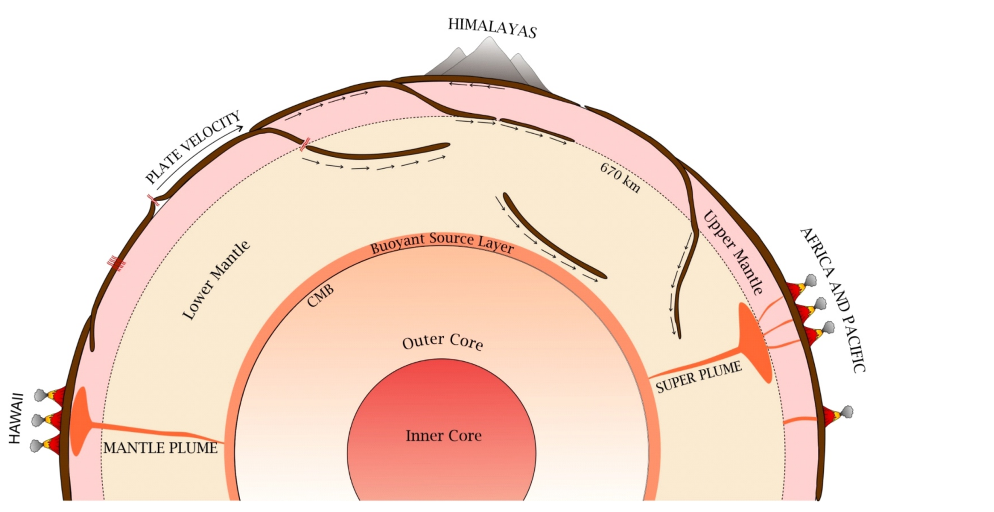

Numerical Modeling: Setup

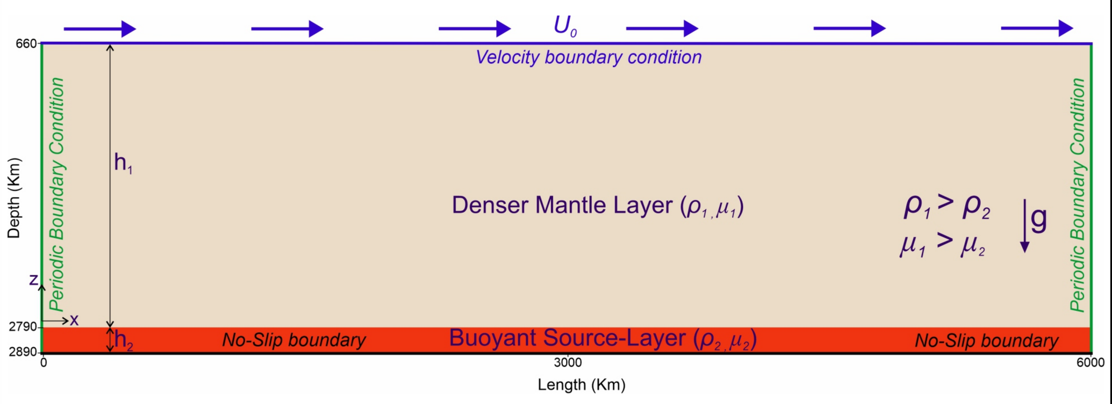

Conservation of Mass and Momentum

$$\nabla \cdot \boldsymbol{u} = 0$$

$$-\nabla P + \nabla.(u_i(\nabla \boldsymbol{u} + \nabla^T \boldsymbol{u})) + \rho_i \boldsymbol{g} = \mathbf{0}$$

Initial Perturbation on the Interface

$$F(y) = h_2 + \Delta A(\cos(kx))$$

h_2= 100 km, ΔA = 0.02 km, λ = 1200 km

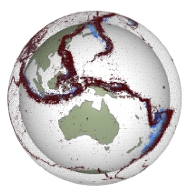

UNDERWORLD2

(Mansour et al., 2020)

http://www.underworldcode.org

@underworldcode

help@underworldcode.org

Particle-in-cell method

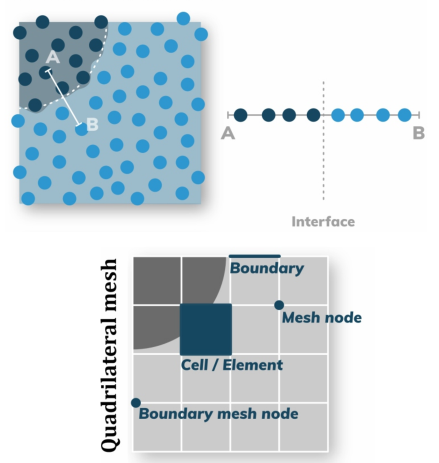

Numerical Modeling: Results

1. Effect of horizontal global flows

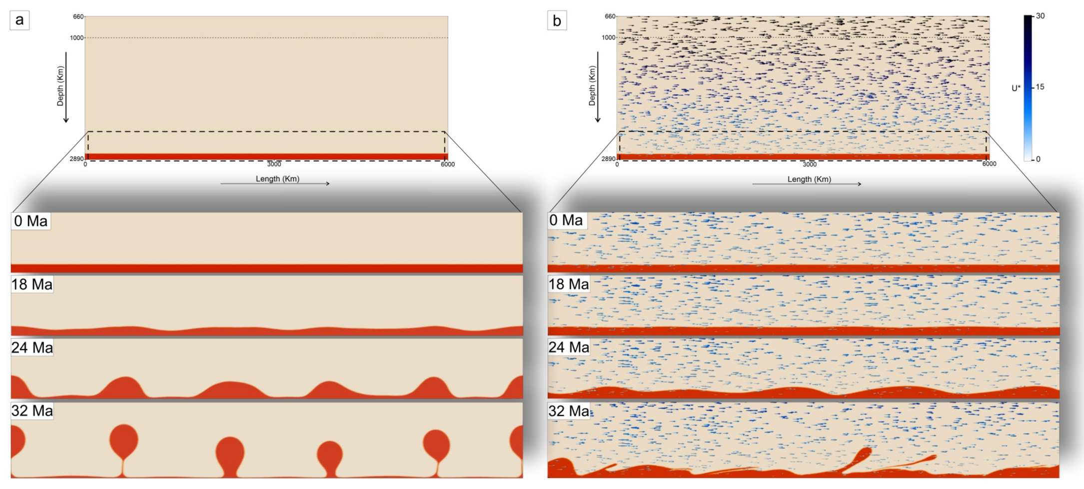

Progressive growth of Rayleigh-Taylor instabilities in CFD model simulations. a) Reference experiment with an initially rest mantle condition (U^*= 0). b) Experiment with an initial horizontal global flow (U^*=36) in the mantle.

2. Role of source-layer buoyancy

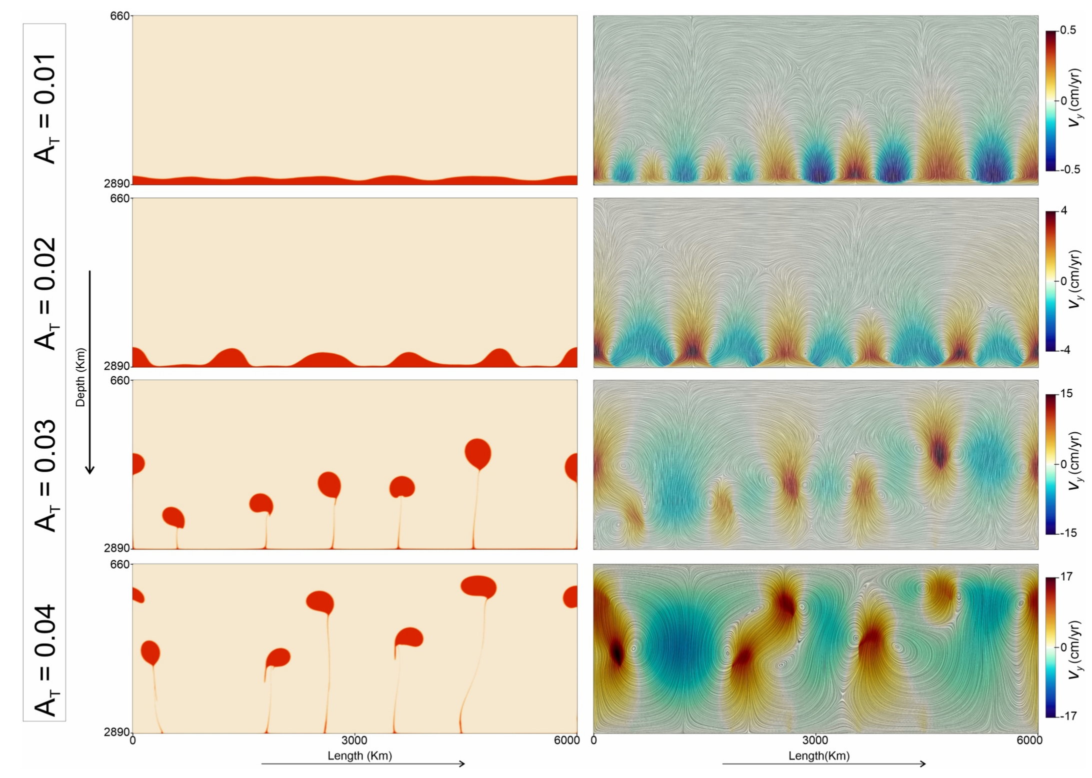

CFD simulations showing the effects of buoyancy factor (A_T) on a) Rayleigh-Taylor instability growth in the buoyant source layers (red colour) and b) the corresponding flow fields represented by streamlines. The colour contours depict the magnitudes of vertical velocity components.

3. Effects of source-layer viscosity

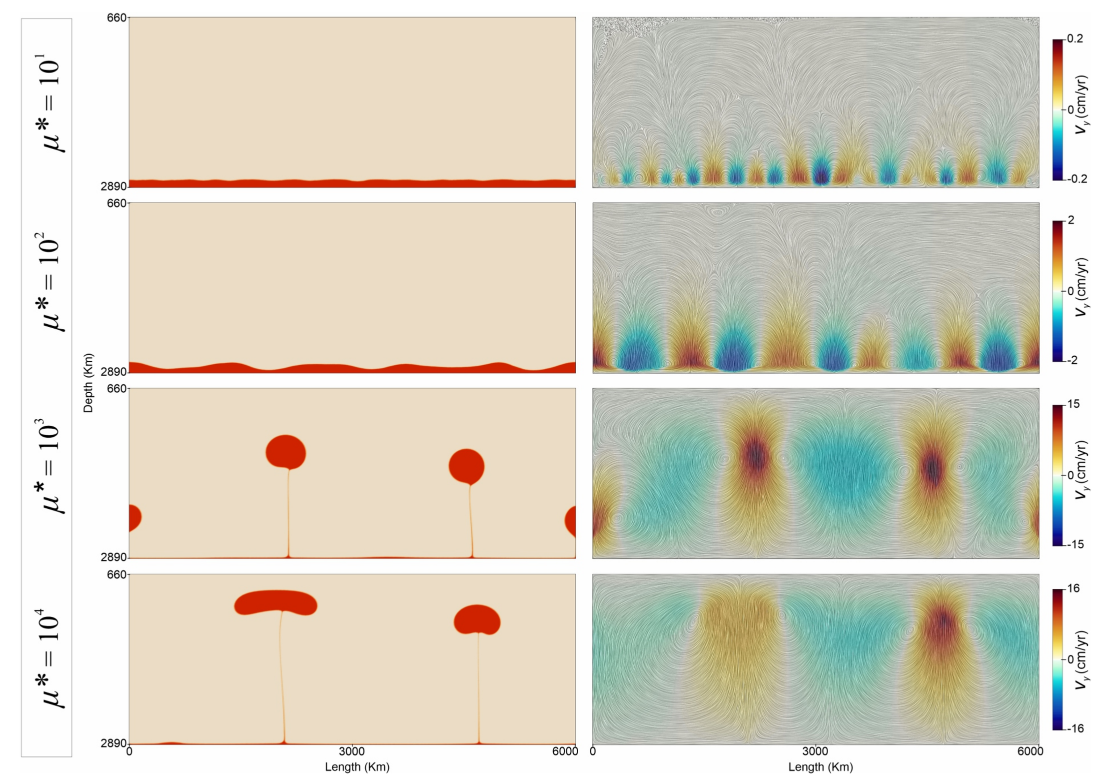

Effects of overburden- to source-layer viscosity (μ^*) on a) Rayleigh-Taylor instability growth and b) the corresponding flow fields in CFD models. The colour contours depict the magnitudes of vertical velocity

Symbol	Physical Meaning
σ	Non-dimensional growth rate
k_M	Characteristic Wavenumber
U	Maximum horizontal flow magnitude at the interface
h_0	Mean height of the interface
μ_2	Fluid viscosity of the thin layer
$\Delta\rho = (\rho_1 - \rho_2)$	Negative density contrast between the two layer
g	Acceleration due to gravity
k	Perturbation wavenumber
μ_1	Fluid viscosity of the overlying layer

Numerical Modeling: Analyses

1. Effect of horizontal global flows

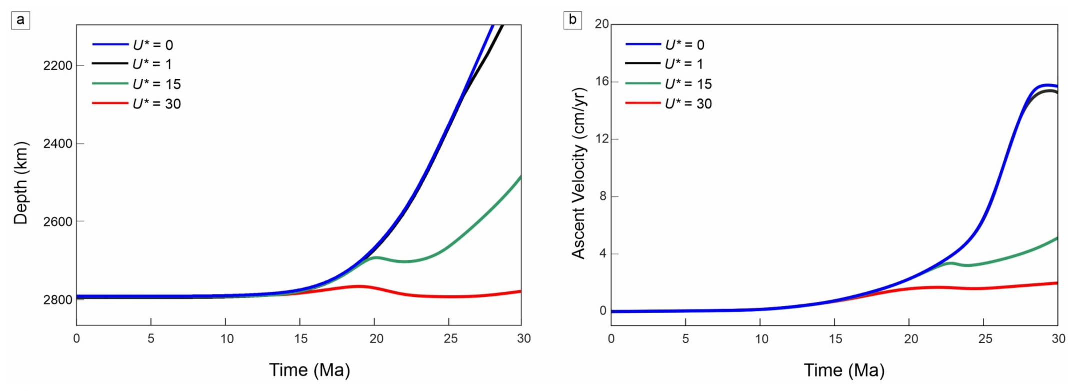

Graphical plots of a) plume ascent heights, and b) vertical ascent velocities of the fastest growing instabilities as a function of time for different normalized global flow-velocity magnitudes (U^*). For this set of simulations, A_T = 0.02 and μ^*= 10^2 .Note that increasing U^* strongly influences the ascent heights and velocities at t > 18 Ma.

2. Role of source-layer buoyancy and source-layer viscosity

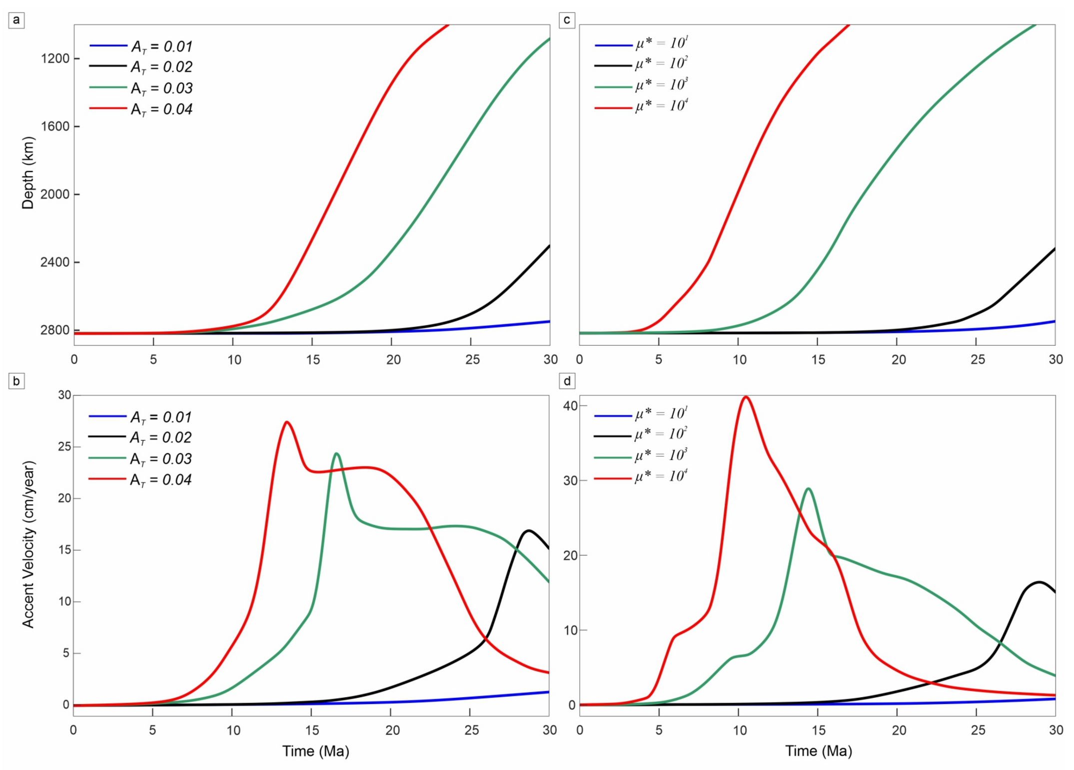

Time series analyses of the plume ascent heights and the vertical ascent velocities of the fastest growing instabilities for different A_T values in a) and b), keeping μ^*= 10^2 and μ^* values in c) and d), keeping A_T = 0.02, respectively.

Theory: Linear Stability Analyses

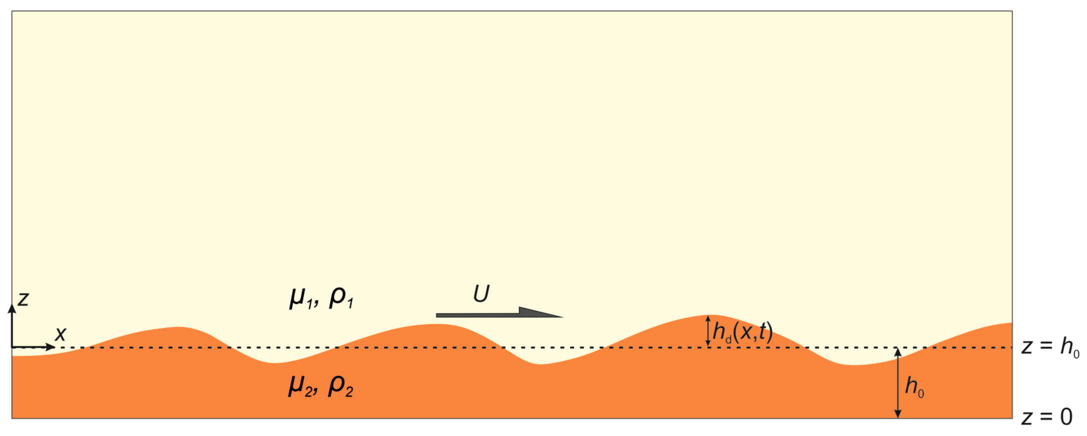

Theoretical consideration for the linear stability analysis: a thin buoyant layer (source layer) (density: ρ_2 and viscosity: μ_2) underlying a denser fluid layer (density: ρ_2 and viscosity: μ_1) (ambient mantle). Dashed and solid lines denote the initial source-layer configuration and the deformed interface geometry formed by RTI. h_o and h_i define the initial source-layer thickness and the vertical deflection at the interface, respectively.

Consideration: Thin Layer Approximation

Eq. of conservation of mass & momentum:

$$\frac{\partial v}{\partial z} + \frac{\partial u}{\partial x} = 0, \qquad \frac{\partial p}{\partial z} = -\Delta\rho g, \qquad \mu_2 \frac{\partial^2 u}{\partial z^2} - \frac{\partial p}{\partial x} = 0.$$

Horizontal velocity (u) component in the thin layer:

$$u = u\big|_{z=h_2} + \frac{1}{2\mu_2}\frac{\partial}{\partial x}\left(-\Delta\rho g h_2 + p\big|_{z=h_2}\right)(z^2 - {h_2}^2).$$

Geometrical evolution of the interface in the presence of a global horizontal flow:

$$\frac{\partial h_2}{\partial t} + \frac{\partial}{\partial x}\left(h_2 u\big|_{z=h_2}\right) - \frac{\partial}{\partial x}\left[\frac{{h_2}^3}{3\mu_2}\frac{\partial}{\partial x}\left(-\Delta\rho g h_2 + p\big|_{z=h_2}\right)\right] = 0.$$

Dispersion relation:

$$\omega = k\,u\big|_{z=h_2} - i\frac{\partial u|_{z=h_2}}{\partial x} + i\frac{h_0^3}{3\mu_2}\Delta\rho g k^2 + i\frac{h_0^2 k_M^2 k U_i}{8}\frac{\mu_1}{\mu_2}\cos\left(\frac{k_M x}{2}\right) - \frac{h_0^2 k_M^2 k U_i}{4}\frac{\mu_1}{\mu_2}\sin\left(\frac{k_M x}{2}\right).$$

Growth rate:

$$\sigma = \frac{k_M U_i}{2}\cos\left(\frac{k_M x}{2}\right) + \frac{h_0^3}{3\mu_2}\Delta\rho g k^2 + \frac{h_0^2 k_M^2 U_i}{8}\frac{\mu_1}{\mu_2}\cos\left(\frac{k_M x}{2}\right).$$

Non-Dimensional Growth rate:

$$\sigma^* = \frac{k_M^* U_i^*}{2}\cos\left(\frac{k_M^* x^*}{2}\right) + \frac{k^{*2}}{3} + \frac{k_M^{*3} U_i^*}{8}\frac{\mu_1}{\mu_2}\cos\left(\frac{k_M^* x^*}{2}\right),$$

$$\sigma^* = \frac{\sigma\mu_2}{\Delta\rho g h_0}, \quad k^* = k h_0$$

Theory: Analyses

1. Effects of horizontal global flows and source-layer viscosity on growth rate

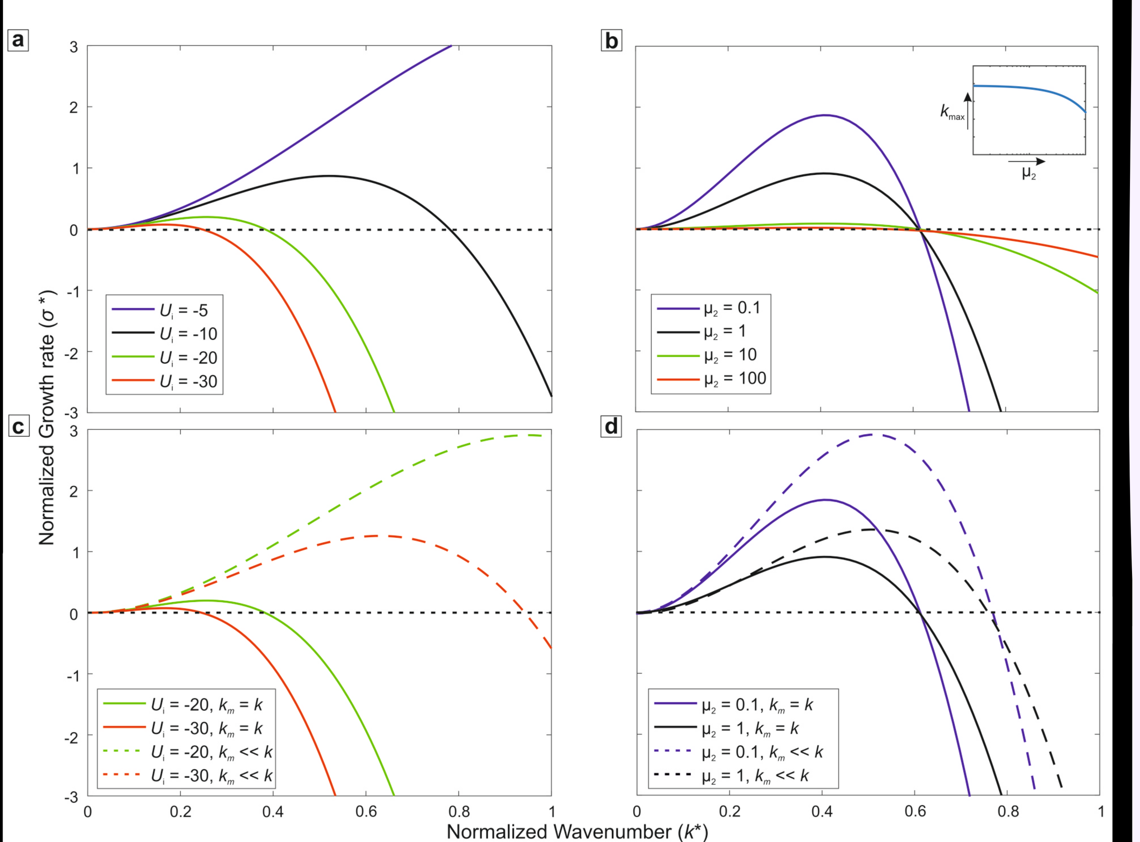

Normalized growth rates (σ^*) versus normalized wavenumber (k^*) plots for different values of (a) the ambient mantle velocity (U_i), and (b) the source layer viscosity (μ_2) obtained from the linear stability analysis for x = 0 (decreasing wavenumber, i.e. increasing wavelength with μ_2 depicted in the inset). Normalized growth rates (σ^*) versus normalized wavenumber (k^*) plots for different values of (c) ambient mantle velocity (U_i), and (d) source layer viscosity (obtained from the linear stability analysis under the condition of $k_M = k$ and $k_M \ll k$.

2. Effects of horizontal global flows and source-layer viscosity on dominant wavelength.

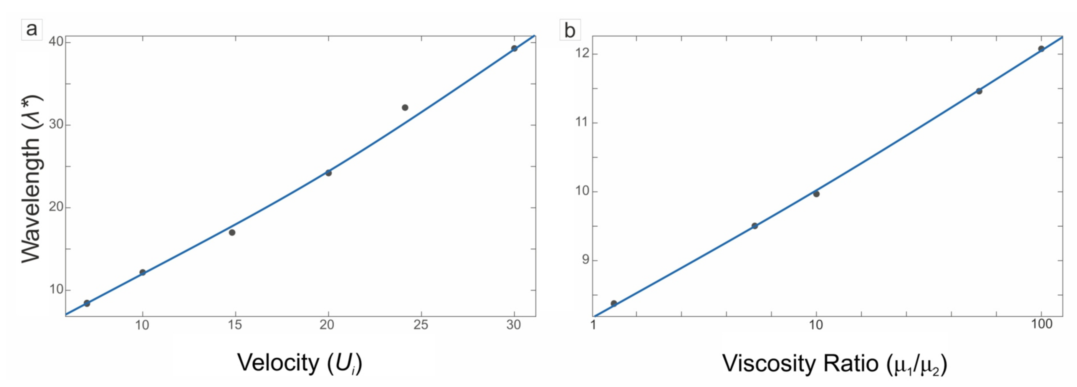

Variations of the instability wavelength (λ^*) with (a) global flow velocity (U_i), and (b) mantle-source layer viscosity ratio (μ_1/μ_2) from the linear stability analysis. All the variables are presented as non-dimensional quantities.

Principle Findings

1. The global flows always dampen the growth of RTIs, where the degree of dampening can vary depending on the initial physical setting of a two-layer system.
2. The linear stability analysis confirms the dampening effects of global flow velocity on the instability growth, predicting that the layer-parallel mantle flow velocities >30 times the initial plume ascent velocity suppress short as well as long-wave instabilities.
3. The analysis also reveals that increasing normalized ambient velocity (10–30) causes the instabilities to increase their dominant wavelengths (10–40), normalized to the initial layer thickness.
4. This work also predicts the effects of additional factors: density ratio, and source-layer viscosity on the growth rate of an instability in an RTI system. All the these parameters act as a driving role in facilitating the instability growth rate.
5. The dampening effects of global flows established in this study can explain the mechanics of plume generation in various geodynamic settings, such as subduction zones and the 660 km transition zone.
6. This study provides a potential explanation for spatially distant primary mantle plumes, manifested in the form of a few hotspots on earth's surface.

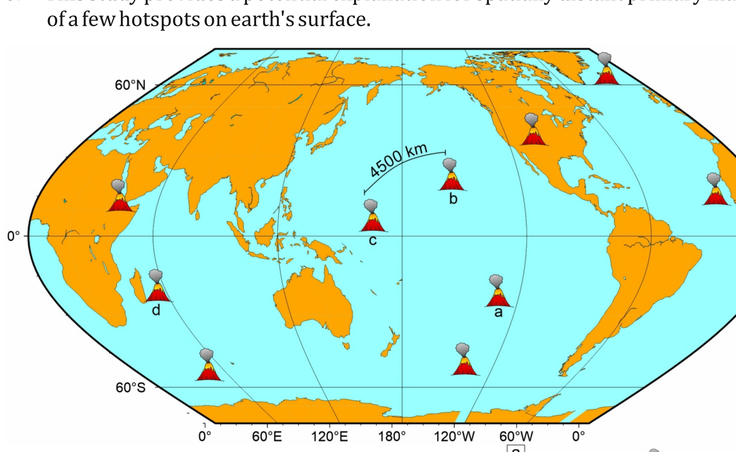

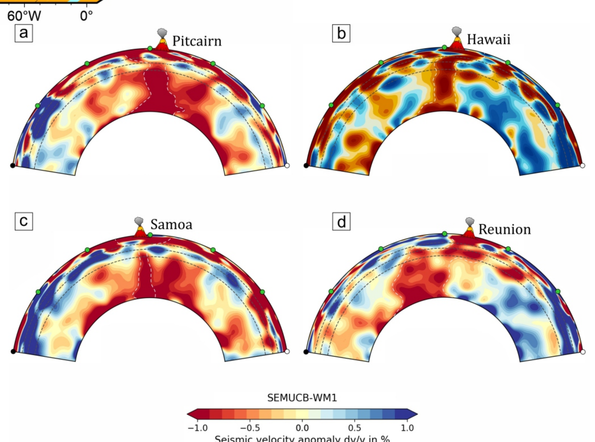

Global distribution of the major hotspots originating from deep-mantle plume sources. The seismic sections show the plume configurations in mantle beneath a) Pitcairn, b) Hawaii, c) Samoa, and d) Afar hotspots. Note that inter-hotspot distances are several thousand kilometres.

References

1. Arnab Roy, Dip Ghosh, Nibir Mandal, Dampening effect of global flows on Rayleigh-Taylor instabilities: implications for deep-mantle plumes vis-à-vis hotspot distributions, Geophysical Journal International, Volume 236, Issue 1, January 2024, Pages 119–138, https://doi.org/10.1093/gji/ggad414.

2. van Zelst, I., F. Crameri, A.E. Pusok, A.C. Glerum, J. Dannberg, C. Thieulot (2022), 101 geodynamic modelling: how to design, interpret, and communicate numerical studies of the solid Earth, Solid Earth, 13, 583–637, doi:10.5194/se-13-583-2022

3. Hosseini, K., Matthews, K. J., Sigloch, K., Shephard, G. E., Domeier, M., & Tsekhmistrenko, M. (2018). SubMachine: Web-based tools for exploring seismic tomography and other models of Earth's deep interior. Geochemistry, Geophysics, Geosystems, 19, 1464–1483. https://doi.org/10.1029/2018GC007431.

4. Bredow, E., Steinberger, B., Gassmöller, R. & Dannberg, J., 2017. How plume-ridge interaction shapes the crustal thickness pattern of the Réunion hotspot track. *Geochemistry, Geophysics, Geosystems*, **18**, 2930–2948. doi:10.1002/2017GC006875

About Us

High Pressure Temperature Laboratory

Publication Link

http://www.jugeodynamics.org

Funding:

1. CSIR, India (09/096(0940)/2018- EMR-I)

2. UGC, India and DST, India .

3. This work used the ARCHER2 UK (https://www.archer2.ac.uk).

4. The DST-SERB, J.C. Bose fellowship (SR/S2/JCB-36/2012).